Cleberton Correia Santos
(Organizador)

Estudos Interdisciplinares nas Ciências e da Terra e Engenharias

Atena
Editora
Ano 2019

Cleberton Correia Santos
(Organizador)

Estudos Interdisciplinares nas Ciências Exatas e da Terra e Engenharias

Atena Editora
2019

Editora Executiva: Profª Drª Antonella Carvalho de Oliveira
Diagramação: Natália Sandrini
Edição de Arte: Lorena Prestes
Revisão: Os Autores

Atena Editora
Ano 2019

Dados Internacionais de Catalogação na Publicação (CIP)
(eDOC BRASIL, Belo Horizonte/MG)

E82 Estudos interdisciplinares nas ciências exatas e da terra e engenharias 1 [recurso eletrônico / Organizador Cleberton Correia Santos. – Ponta Grossa, PR: Atena Editora, 2019. – (Estudos Interdisciplinares nas Ciências Exatas e da Terra e Engenharias; v. 1)

Formato: PDF
Requisitos de sistema: Adobe Acrobar Reader
Modo de acesso: World Wide Web
Inclui bibliografia
ISBN 978-85-7247-621-8
DOI 10.22533/at.ed.218191109

1. Ciências exatas e da Terra. 2. Engenharias. 3. Tecnologia. I.Santos, Cleberton Correia. II. Série.

CDD 016.5

Elaborado por Maurício Amormino Júnior – CRB6/2422

Atena Editora
Ponta Grossa – Paraná - Brasil
www.atenaeditora.com.br
contato@atenaeditora.com.br

Atena Editora
Ano 2019

APRESENTAÇÃO

O livro "**Estudos Interdisciplinares nas Ciências Exatas e da Terra e Engenharias**" de publicação da Atena Editora apresenta em seu primeiro volume 35 capítulos relacionados temáticas de área multidisciplinar associadas à Educação, Agronomia, Arquitetura, Matemática, Geografia, Ciências, Física, Química, Sistemas de Informação e Engenharias.

No âmbito geral, diversas áreas de atuação no mercado necessitam ser elucidadas e articuladas de modo a ampliar sua aplicabilidade aos setores econômicos e sociais por meio de inovações tecnológicas. Neste volume encontram-se estudos com temáticas variadas, dentre elas: estratégias regionais de inovação, aprendizagem significativa, caracterização fitoquímica de plantas medicinais, gestão de riscos, acessibilidade, análises sensoriais e termodinâmicas, redes neurais e computacionais, entre outras, visando agregar informações e conhecimentos para a sociedade.

Os agradecimentos do Organizador e da Atena Editora aos estimados autores que empenharam-se em desenvolver os trabalhos de qualidade e consistência, visando potencializar o progresso da ciência, tecnologia e informação a fim de estabelecer estratégias e técnicas para as dificuldades dos diversos cenários mundiais.

Espera-se com esse livro incentivar alunos de redes do ensino básico, graduação e pós-graduação, bem como pesquisadores de instituições de ensino, pesquisa e extensão ao desenvolvimento estudos de casos e inovações científicas, contribuindo então na aprendizagem significativa e desenvolvimento socioeconômico rumo à sustentabilidade e avanços tecnológicos.

Cleberton Correia Santos

SUMÁRIO

CAPÍTULO 28

INVESTIGAÇÃO ESTRUTURAL, MORFOLÓGICA E FOTOCATALÍTICA DE MICROCRISTAIS DE β-$(AG_{2-2X}ZN_X)MoO_4$

Fabiana de Sousa Cunha
PPGQ-CCN-DQ-DF-GERATEC, Universidade Estadual do Piauí, Rua: João Cabral, N. 2231, P.O. Box 381, CEP: 64002-150, Teresina, PI, Brazil

fabianadesousa3@gmail.com

Francisco Henrique Pereira Lopes
PPGQ-CCN-DQ-DF-GERATEC, Universidade Estadual do Piauí, Rua: João Cabral, N. 2231, P.O. Box 381, CEP: 64002-150, Teresina, PI, Brazil

henriquethe.11@gmail.com

Amanda Carolina Soares Jucá
PPGQ-CCN-DQ-DF-GERATEC, Universidade Estadual do Piauí, Rua: João Cabral, N. 2231, P.O. Box 381, CEP: 64002-150, Teresina, PI, Brazil

Lara Kelly Ribeiro da Silva
DQ-UFSCar, Universidade Federal de São Carlos, P.O. Box 676, CEP: 13565-905, São Carlos, SP, Brazil

Keyla Raquel Batista da Silva Costa
UFPI, Universidade Federal do Piauí - Bairro Ininga, CEP: 64049-550, Teresina, PI, Brasil.

Júlio César Sczancoski
DQ-UFSCar, Universidade Federal de São Carlos, P.O. Box 676, CEP: 13565-905, São Carlos, SP, Brazil

Francisco Eroni Paz dos Santos
UFPI, Universidade Federal do Piauí - Bairro Ininga, CEP: 64049-550, Teresina, PI, Brasil.

Elson Longo
DQ-UFSCar, Universidade Federal de São Carlos, P.O. Box 676, CEP: 13565-905, São Carlos, SP, Brazil

Laécio Santos Cavalcante
PPGQ-CCN-DQ-DF-GERATEC, Universidade Estadual do Piauí, Rua: João Cabral, N. 2231, P.O. Box 381, CEP: 64002-150, Teresina, PI, Brazil

Gustavo Oliveira de Meira Gusmão
PPGQ-CCN-DQ-DF-GERATEC, Universidade Estadual do Piauí, Rua: João Cabral, N. 2231, P.O. Box 381, CEP: 64002-150, Teresina, PI, Brazil

RESUMO: Neste capítulo de livro, nós relatamos sobre a estrutura, morfológia e as propriedades fotocatalíticas dos microcristais de molibdato de prata e zinco [β-$(Ag_{2-2x}Zn_x)MoO_4$] com as seguintes concentrações (x = 0; 0,01; e 0,02) sintetizados pelo método de injeção de íons em uma solução quente a 90 ºC em 1 minuto com rápido resfriamento por imersão em banho de gelo. Estes microcristais foram caracterizados estruturalmente por difração de raios-X (DRX) e refinamento Rietveld. O comportamento óptico foi investigado por espectroscopia ultravioleta-visível (UV-Vis) à temperatura ambiente. As morfologias foram observadas por meio de microscopia eletrônica de varredura por emissão de campo (MEVEC). As propriedades

fotocatalíticas para degradação do corante Rodamina B foram realizadas empregando quatro lâmpadas de UV (λ_{max} = 254 nm). Os padrões de DRX e refinamento Rietveld indicam que todos os microcristais de β-$(Ag_{2-2x}Zn_x)MoO_4$ apresentam estrutura cúbica do tipo espinélio. Os espectros de UV-Vis indicaram que o aumento da concentração molar de Zn promove um ligeiro decrécimo no valor de banda proibida. As imagens of FE-SEM mostram uma modificação na forma, bem como o aparecimento de várias faces e poros na superfície dos cristais. Finalmente, nós demonstramos que a atividade fotocatalítica pode ser aumentada até 120 min com aproximadamente 99,99% para a degradação do corante Rodamina B usando os microcristais de β-$(Ag_{2-2x}Zn_x)MoO_4$ com (x = 0.01) como fotocatalisador.
PALAVRAS-CHAVE: Microcristais de β-$(Ag_{2-2x}Zn_x)MoO_4$; Dados de Refinamento Rietveld; Banda proibida; Atividade Fotocatalítica

TITLE: STRUCTURAL, MORPHOLOGICAL AND PHOTOCATALYTIC INVESTIGATION OF β-$(AG_{2-2X}ZN_X)MoO_4$ MICROCRYSTALS

ABSTRACT: In this chapter of the book, we report about the structure, morphology and photocatalytic properties of silver and zinc molybdate [β-$(Ag_{2-2x}Zn_x)MoO_4$] microcrystals with the following concentrations (x = 0, 0.01, and 0.02) synthesized by the ions injection method in a hot solution at 90 ºC in 1 minute with fast cooling by immersion in an ice bath. These microcrystals were characterized structurally by X-ray diffraction (XRD) and Rietveld refinement. The optical behavior was investigated by ultraviolet-visible (UV-Vis) spectroscopy at room temperature. The morphologies were observed by means of field emission scanning electron microscopy (FE-SEM). The photocatalytic properties for rhodamine B dye degradation were performed using four UV lamps (λ_{max} = 254 nm). The XRD patterns and Rietveld refinement patterns indicate that all [β-$(Ag_{2-2x}Zn_x)MoO_4$ microcrystals have a spinel-type cubic structure. The UV-Vis spectra indicated that the increase in the molar concentration of Zn promotes a slight decrease in the band gap value. FE-SEM images show a change in shape as well as the appearance of several faces and pores on the surface of the crystals. Finally, we demonstrated that the photocatalytic activity can be increased up to 120 min with approximately 99.99% for the degradation of the Rhodamine B dye using the β-$(Ag_{2-2x}Zn_x)MoO_4$ microcrystals with (x = 0.01) as a photocatalyst.
KEYWORDS: β-$(Ag_{2-2x}Zn_x)MoO_4$ microcrystals; Rietveld Refinement data; Band gap; Photocatalytic Activity

1 I INTRODUCTION

In the past years, crystals and ceramics of silver molybdate (Ag_2MoO_4) were initially prepared by different synthesis methods, such as oxides mixture or solid state reaction (WENDA, E., 1990; WENDA, E., 1998; SUTHANTHIRARJ, S.A.; PREMCHAND, Y.D., 2004), precipitation with calcination at high temperature (ROCCA,

F. et al, 1999), and by crystal growth by the so-called “Czochralski” (BROWN, S.; MARSHALL, A.; HIRST, P., 1993). However, all these synthetic methods require high temperature, pressure thermodynamics, long processing times, low reaction kinetics, and sophisticated equipment with expensive financial costs for the teaching and research center. Furthermore, these synthesis methods of obtention of Ag_2MoO_4 crystals can induce the formation of deleterious or secondary phases and produce powder/crystals of non-homogeneous shape and size.

In recent years, various synthesis methods have been developed and used in the preparation of Ag_2MoO_4 micro- and nanocrystals (KOKULNATHAN, T. et al, 2019; WU, M. et al, 2018). These preparation methods can overcome the problems encountered in older synthetic methods and may also facilitate crystals with pure phase, size and controlled form. The different methods of synthesis that have been reported in the literature to obtain the Ag_2MoO_4 crystals are controlled precipitation (RAO, K.S.; VAIDYA, V.G., 1975; RICCI, J.E.; LINKE, W.F., 1951) and conventional hydrothermal (CH) (CUI, X. et al, 2004; SINGH, D.P. et al, 2012) and microwave-hydrothermal (MH) (LI, Z.Q.; CHEN, X.T.; XUE, Z.L., 2013). In particular, the CH method has been recently used in the preparation of several molybdates with different shapes and sizes (LI, L. et al, 2014; TAWDE, D.; SRINIVAS, M.; MURTHY, K.V.R., 2011; WANG, X.F. et al, 2014). Therefore, the CH and MH methods have received a lot of attention from the scientific community due to its numerous advantages over the older conventional methods, such as the use of non-toxic solvent to the environment (water) and low processing temperatures (≤ 200 ºC) (TIAN, G.; SUN, S., 2011; SCZANCOSKI, J.C. et al, 2008).

According to the literature (LEI, F. et al, 2009; SOMIYA, S.; ROY, R., 2000), the CH method is defined with a processing method for obtaining crystalline materials from aqueous solution-soluble or dissolved reagents or with the use of mineralizers as chemical bases [hydroxide (NaOH) and potassium hydroxide (KOH)] under temperature (³ 100 ºC) and pressure (≥ 1.0 atm). Generally, the materials oxide obtained by this synthesis method are very fine, crystalline and easily dispersed in several solvents (KOMARNENI, S.; ROY, R.; LI, Q.H., 1992). Recently, the CH method has been reported in the literature (CUI, X. et al, 2004) for the preparation of Ag_2MoO_4 and $Ag_2Mo_2O_7$ crystals. However, to obtain these crystals by this method, long processing times (12-24 h) were required due to the low reaction kinetics (HASHIM, M. et al, 2011).

Recently, (FODJO, E.K. et al, 2013) prepared very fine Ag_2MoO4 powders by the homogeneous precipitation method at 80 ºC (pH = 8) assisted by HC processing for 3 h with possible applications as substrate for Raman scattering improvement. In another work, (GOUVEIA, A.F. et al., 2014) performed a theoretical and experimental text about the electronic structure and photoluminescent properties of Ag_2MoO_4 microcrystals of different sizes and shapes. In addition, (FABBRO, M.T. et al, 2016) prepared microcrystals of Ag_2MoO_4 by the precipitation method with different solvents

(water, ethanol and ammonia) and investigated their optical and antifungal properties as: broom and flower by HC method at different pH ranges. Very recently, (NG, C.H.B.; FAN, W.Y., 2017) have prepared β-Ag_2MoO_4 concave and convex crystals with high-index facets by the controlled precipitation between $AgNO_3$ and Na_2MoO_4 in aqueousmedia.

In addition, the literature has reported (LI, Z.Q.; CHEN, X.T.; XUE, Z.L., 2013; CUTRONI, M. et al. 1998; MANDANICI, A. et al, 2009; JUAREZ, J.C.; MORALES, R., 2008; BAI, Y.Y.; LU, Y.; LIU, J.K. J., 2016; LIU, E. et al, 2013), thermal expansion, ionic conductivity and electrical properties of the system (AgI-Ag_2MoO_4), investigations on the coefficient of friction and reduction mechanisms of Ag_2MoO_4 to obtain Ag and Mo with hydrogen gas, on the photocatalytic activity of the Ag-Ag_2MoO_4 and Ag @ Ag_2MoO_4-AgBr crystals for degradation of organic dyes rhodamine B, bromophenol blue and starch 10B using visible light and also with synergistic lubricating action.

In relation to the modification of the *A*-site in the Ag_2MoO_4 crystals, one work in the literature has been found to dope with 1% of rare-earth (Eu^{3+}) ions (GUPTA, S.K. et al, 2015). However, very recently (COIMBRA, D.W.R. et al, 2019) has reported in the literature the modification the *A*-site of β-Ag_2MoO_4 microcrystals with the Zn^{2+} ions and investigating their structure, morphology and photocatalytic properties for degradation of Remazol Brilliant Violet 5R (RBV5R) anionic dye, which were synthesized by the sonochemical method at 30 ºC for 3 h.

In relation to the crystalline structure, the molybdates ($AMoO_4$; A^{2+} = Ca, Sr, Ba, and Pb) has a scheelite-type tetragonal structure and characterized by presenting a space group ($I4_1/a$) (RYU, J.H. et al, 2005; GONG, Q. et al, 2006; MARQUES, A.P.A. et al, 2006; BI, J. et al, 2009; WANG, W.S. et al, 2009). Meanwhile, the molybdates ($AMoO_4$; A_{2+} = Mn, Fe, Co, Ni, Cu e Zn) formed by transition elements (d-block) exhibit a wolframite-type tetragonal structure with space group ($P2/c$) or a triclinic structure with phase alpha (a) and space group (P) (ABRAHAMS, S.C.; REDDY, J.M., 1965; YADAVA, Y.P.; SINGH, R.A., 1986; SMITH, G.W.; IBERS, J.A., 1965; THÉODET, M. et al, 2016; SMITH, G.W.; IBERS, J.A., 1965; SOUZA, E.L.S. et al, 2014; CAVALCANTE, L.S. et al, 2013). Therefore, both scheelite and wolframite types obey a general chemical formula ($AMoO_4$), since they are composed of bivalent (A^{2+}) cations and molybdate (MoO_4^{2-}) complex ions in aqueous solution. The scheelite-type tetragonal structure is formed by following clusters coordination, the A^{2+} are deltahedral [AO_8] clusters and Mo are tetrahedral [MoO_4] clusters, while the wolframite-type tetragonal structure is formed by octahedral [AO_6] clusters and octahedral [MoO_6] clusters both as a solid solution, respectively. However, the Ag_2MoO_4 crystal may be formed in aqueous solution from monovalent cations silver ions (Ag^+). Thus, 2 moles of Ag^+ ions is required for 1 mol of complex ions, which must be presents in aqueous solution to form the solid phase of this crystal.

The Ag_2MoO_4 crystals presents two types of electronic structure, depending on the pressure conditions under which the crystal is subjected (ARORA, A.K.

et al, 2012).At room temperature, Ag_2MoO_4 crystal exhibits a beta-phase (β) is related to spinel-type cubic structure, which is more stable in nature over ambient conditions. However, when subjected to high hydrostatic pressures, these crystals have a tetragonal structure associated with the alpha (α) phase that is metastable. Therefore, there may be two types of crystals one stable β-Ag_2MoO_4 phase and another α-Ag_2MoO_4 metastable (BELTRÁN, A. et al, 2014). Recently, the literature (NG, C.H.B.; FAN, W.Y., 2015) has reported the formation of metastable α-Ag_2MoO_4 crystals by the solution phase precipitation method under environmental conditions using different amounts of the [3-bis (2-pyridyl) pyrazine] dopant. In addition to this work, Moura et al. Investigated that a first-order phase transition with an increase in temperature around 268 ºC of the cubic structure related to phase-β to an unknown structure can occur (MOURA, J.V.B. et al, 2016).

Figure 1 illustrates the schematic representation of our unit cell for spinel-type cubic structure of the β-Ag_2MoO_4 microcrystal prepared by method of ion injection in a hot solution at 90 ° C in 1 minute with fast cooling by immersion in an ice bath and modeled from the structural refinement data by the Rietveld method reported in the literature (CUNHA, F.S. et al, 2015).

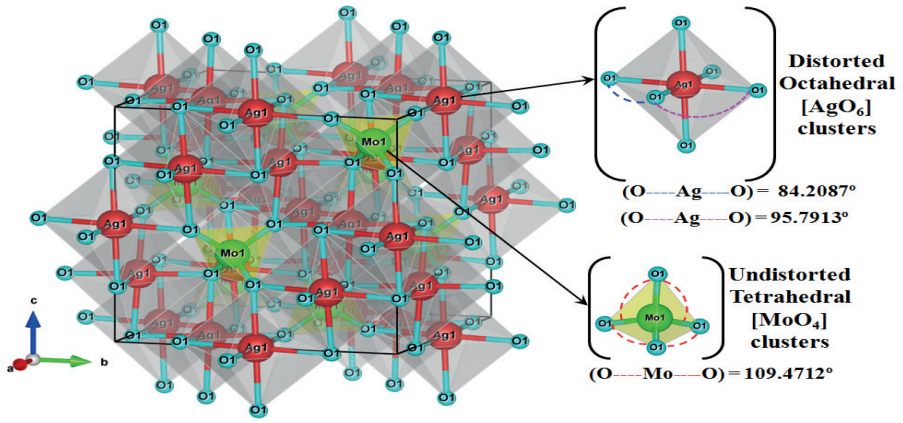

Figure 1: Schematic representation of the unit cell of the β-Ag2MoO4 crystals with their respective cluster coordination.

The unit cell for the β-Ag_2MoO_4 crystals shown in Figure 1 can be modeled using the VESTA program version 3.4.6 for Windows-7 (MOMMA, K.; IZUMI, F., 2008; MOMMA, K.; IZUMI, F., 2011) using the lattice parameter data and atomic positions obtained from the Rietveld method (RIETVELD, H.M., 1967; RIETVELD, H.M., 1969). The β-Ag_2MoO_4 crystals have a cubic structure with a space group ($Fd\bar{3}m$), with symmetry point group (O_h^7) and eight molecules per unit cell (Z = 8) (WYCKOFF, R.W.G. J., 1922). In this cell the O-Ag-O and O-Mo-O bonds were designed out of unit cell. It can be observed in Figure 1 that all the molybdenum atoms (Mo) are coordinated to four oxygen atoms forming distorted tetrahedral [MoO_4] clusters. These polyhedra have a tetrahedral configuration with symmetry point group (T_d) formed by (4 vertices, 4 faces, and 6

edges), while all the silver atoms (Ag) are coordinated by six oxygen atoms forming distorted octahedral [AgO_6] clusters. These octahedral polyhedra have a symmetry point group (O_h) formed by (6 vertices, 8 faces, and 12 edges). All octahedral [AgO_6] clusters are distorted into the crystal lattice promotion the break of high symmetry at β-Ag_2MoO_4 cubic structure. All octahedral [AgO_6] clusters are distorted into the crystal lattice promotion the breaking of high symmetry for β-Ag_2MoO_4 cubic structure. These differences in the (O-Ag-O) and/or (O-Mo-O) bonding angles may lead to different levels of order-structural disorder or distortions in the lattice of this crystal.

In general, the literature has focused their works and investigations for the photocatalytic properties of pure and/or modified β-Ag_2MoO_4 crystals with the addition of other photocatalytic compounds (oxides and graphene) in the visible region. Therefore, the present book chapter has as the main objective synthesize the pure and modified [β-($Ag_{2-2x}Zn_x$)MoO_4] microcrystals with the following concentrations (x = 0, 0.01, and 0.02) by a new method of synthesis. These crystals were synthesized by the ions injection method in a hot solution at 90 ºC in 1 minute with fast cooling by immersion in an ice bath. Moreover, all the microcrystals were structurally characterized by means of X-ray diffraction (XRD) and Rietveld refinement analyses. The optical behavior was investigated by ultraviolet-visible (UV-Vis) spectroscopy at room temperature. The shape and average crystal sized were observed by field emission electron microscopy (FE-SEM). Finally, the photocatalytic activity properties for degradation of rhodamine B (RhB) and methylene blue dyes were performed by using four UV lamps (18 W each).

2 I EXPERIMENTAL PROCEDURE

2.1 Synthesis Method

The experimental procedure of synthesize the pure and modified [β-($Ag_{2-2x}Zn_x$) MoO_4] microcrystals with the following concentrations (x = 0, 0.01, and 0.02) by the ion injection method in a hot solution at 90 ºC in 1 minute with fast cooling by immersion in an ice bath. In the first step, 1×10^{-3} moles of sodium molybdate dihydrate ($Na_2MoO_4.2H_2O$; 99.5% purity; Sigma-Aldrich®) was dissolved in deionized in 50 mL of deionized water at 90 ºC. In the second step, 1×10^{-3} moles of silver nitrate ($AgNO_3$; 99.0% purity, Sigma–Aldrich®) for obtain the pure β-Ag_2MoO_4 microcrystals. In the third step, the modified [β-($Ag_{2-2x}Zn_x$)MoO_4] microcrystals with (x = 0.01, and 0.02) or x.mols(%) of zinc nitrate hexahydrate ($Zn(NO_3)_2.6H_2O$; 99.0% purity, Sigma–Aldrich) were dissolved separately in deionized water. In following, both the aqueous solution containing the $x.Ag^+$ and $x.Zn^{2+}$ ions were mixed in a plate at 90 ºC under stirring at 380 rotations per minute (RPM). In the fourth step, the $x.Ag^+$ and $x.Zn^{2+}$ ions were sucked for the interior of a syringe and rapidly injected to the molybdate (MoO^{2-}_4) complex ions in aqueous solution. Finally, this white suspension this system was

immediately transferred to a plastic becker containing 100 mL deionized water with cubes ice, which later it was taken to the refrigerator staying in this one during 24 hours. After this time in the refrigerator, a precipitate of beige coloration was obtained in suspension. After 10 cycles of washes in an Eppendorf® centrifuge (model 5804) at 8,000 RPM for 10 min, in each cycle. Finally, the precipitates were dried at 65 ° C for 10 hours in a muffle furnace (model EDG3000/3P) with a heating rate of 5 ºC/min. These procedures were performed for all four concentrations.

2.2 Characterizations

The structural analysis of [β-($Ag_{2-2x}Zn_x$)MoO_4] microcrystals with the following concentrations (x = 0, 0.01, and 0.02) was performed by means of XRD patterns and Rietveld refinement analysis by using a D/Max-2500PC diffractometer (Rigaku, Japan) with CuKα radiation. These data were collected over 2θ ranging from 10° to 80° in normal routine and over 2θ ranging from 10° to 110° in Rietveld routine both with a scanning scan rate and step size of 0.2°/min and 0.02°, respectively. The shapes and sizes of these [β-($Ag_{2-2x}Zn_x$)MoO_4] microcrystals were observed using a Supra 35-VP field-emission scanning electron microscope (FE-SEM) (Carl Zeiss, Germany) operated at 5 kV. UV-Vis spectroscopy was performed using a Shimadzu® spectrophotometer (model UV-2600, Japan) in the 200-800 nm wavelength range to obtain diffuse reflectance spectra.

2.3 Photocatalytic Activity Measurements

The photocatalytic (PC) activity of these β-($Ag_{2-2x}Zn_x$)MoO_4 microcrystals for degradation of [9-(2-carboxyphenyl)-6-diethylamino-3-xanthenylidene]-diethylammonium chloride, which is known as tetraethylated rhodamine or Rhodamine B dye (RhB; $C_{28}H_{31}ClN_2O_3$, 95% purity, Sigma–Aldrich®, USA) with colour index number (CI. 45170) inaqueous solution were tested under UV-light. 50 mg of β–($Ag_{2-2x}Zn_x$)MoO_4 microcrystals with different (x = 0; 0.01; and 0.02) as a catalyst were placed in 250 mL beakers, and 50 mL of the RhB dye solution (1×10^{-5} mol.L^{-1}; pH = 6.25). The suspensions were ultrasonicated initially for 30 min in an ultrasonic cleaner (1510 DTH Branson®, CPX1800H model, USA) with a frequency of 40 kHz before illumination and then stored in the dark for 2 min to allow the saturated absorption of RhB dye solutions onto the catalyst. The beakers were then placed in a photo-reactor at 25 ºC, kept inside the ultrasound bath switched on and illuminated by four UV-C lamps (Moran Ligth® model, USA) with power of 18 W each, the luminosity of 145 lumens, beam angle at 320º and maximum intensity at 254 nm the source with the distance about 45 cm of the surface dye solution. At ten-minute intervals, a 3 mL aliquot was removed and centrifuged at 8,500 rpm for 10 min to remove the nanocrystals from the suspension. The following equation (1) was used to calculate the colour removal efficiency of RhB dye:

$$\text{Efficiency of catalyst } [\beta\text{–}(Ag_{2-2x}Zn_x)MoO_4]\% = \frac{C_0 - C_t}{C_0 \times 100} \quad (1)$$

where, C_0 is the concentration of RhB dye solution at initial and C_t is the concentration of the RhB dye solution at the time *t*, respectively.

Finally, variations in the absorption band maximum of the supernatant solutions were monitored by means of UV-Vis spectroscopy using a double-beam spectrophotometer with a double monochromator and a photomultiplier tube detector of Shimadzu Scientific Instruments (UV-2600 model, Japan).

3 I RESULTS AND DISCUSSION

3.1 XRD Patterns Analysis

The Fig. 2(a-c) illustrates the XRD patterns of β-$(Ag_{2-2x}Zn_x)MoO_4$ microcrystals with (x = 0; 0.01; and 0.02) prepared by the ions injection method in a hot solution at 90 ºC in 1 minute with fast cooling by immersion in an ice bath, respectively.

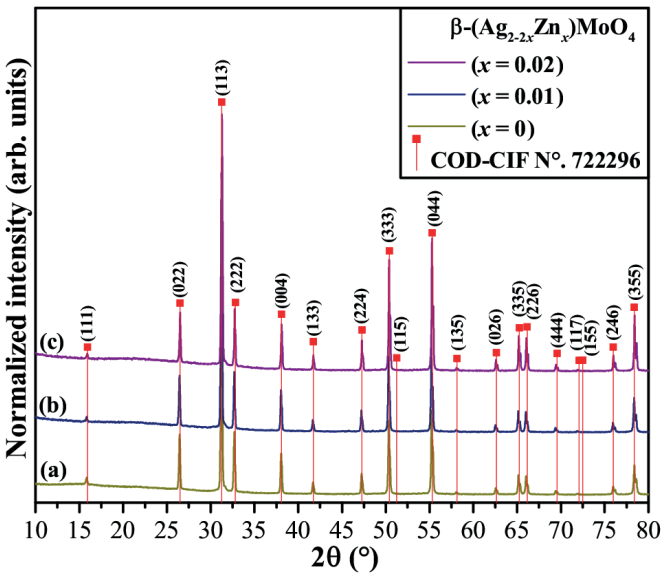

Fig. 2: Normalized XRD patterns of β-$(Ag_{2-2x}Zn_x)MoO_4$ microcrystals with (a) x = 0; (b) x = 0.01; and (c) x = 0.02; synthesized by the ions injection method at 90 ºC for 1 min, respectively.. The vertical lines (I) indicate the respective positions and intensities found in COD-CIF card Nº. 722296 corresponding to the cubic β-Ag_2MoO_4 phase.

According to the literature (FIGUEIREDO, A.T. et al, 2006), the degree of structural order-disorder at long-range or the periodicity of crystalline lattice for β-$(Ag_{2-2x}Zn_x)MoO_4$ microcrystals with different (x) amount in moles of Zn atoms at the *A*-site replacing Ag atoms was verified by the XRD technique (COIMBRA, D.W.R. et al, 2019). As it can be observed in XRD patterns displayed in Fig. 2(a–c), all our microcrystals present XRD peaks sharp and well-defined, in this way it's possible attributed to a

good degree of structural order at long-range. All our XRD patterns can be indexed exactly to a spinel-type cubic structure with space group (*Fd3m*) and with symmetry point group (O^7_h) (SUDARSHAN, S.S. et al, 2019). Moreover, any diffraction peaks related to silver oxide (Ag_2O) or reduced silver (Ag^0) nanoparticles were detected (WANG, P. et al, 2009). We can clearly observe that all XRD peaks can be indexed and purchased with results reported in Crystallography Open Database (COD) and crystallographic information file (CIF) base Nº. 722296 (WANG, X.F. et al, 2014) and recentes papers reported in the literature (XUE, Y.N. et al, 2019; JIAO, Z. et al, 2019). To confirm whether the qualitative data observed by means of XRD measurements are very significant. Therefore, we have carried out the structural refinement by the Rietveld method (CUNHA, F.S. et al, 2015) for our β-$(Ag_{2-2x}Zn_x)MoO_4$ microcrystals with (x = 0; 0.01; and 0.02).

It is well known and established in the literature that the quality of a structural refinement also can be verified by the value of R_w values, that is very important. Its absolute value does not depend on the absolute value of the intensities, but it depends on the background. With a high background is more easy to reach very low values. Increasing the number of peaks (sharp peaks) is more difficult to get a good value. As can be observed in Fig. 2(a-c), the replacement of Ag^+ by Zn^{2+} ions into the pure β-Ag_2MoO_4 cubic lattice promoted a small displacement of all diffraction peaks to low 2θ angles. According to Bragg's law (nλ = 2dsinθ), this displacement occurs when there is a change in the lattice parameters (NOGUEIRA, I.C. et al, 2013). The behavior is promoted by the replacement of Ag^+ (ionic radius of 145 pm) by Zn^{2+} (ionic radius of 74 pm), reducing the unit cell volume. In addition, more details quantitative about XRD patterns can be verified in the following 3.2 section from Rietveld refinement data.

3.2 Rietveld refinement analyses

Our structural refinements using the Rietveld refinement method (RIETVELD, H.M., 1967) confirmed that all β-$(Ag_{2-2x}Zn_x)MoO_4$ microcrystals with (x = 0; 0.01; and 0.02) have a spinel-type cubic structure without deleterious or secondary phases, as illustrated in Figs. 3(a–c), respectively.

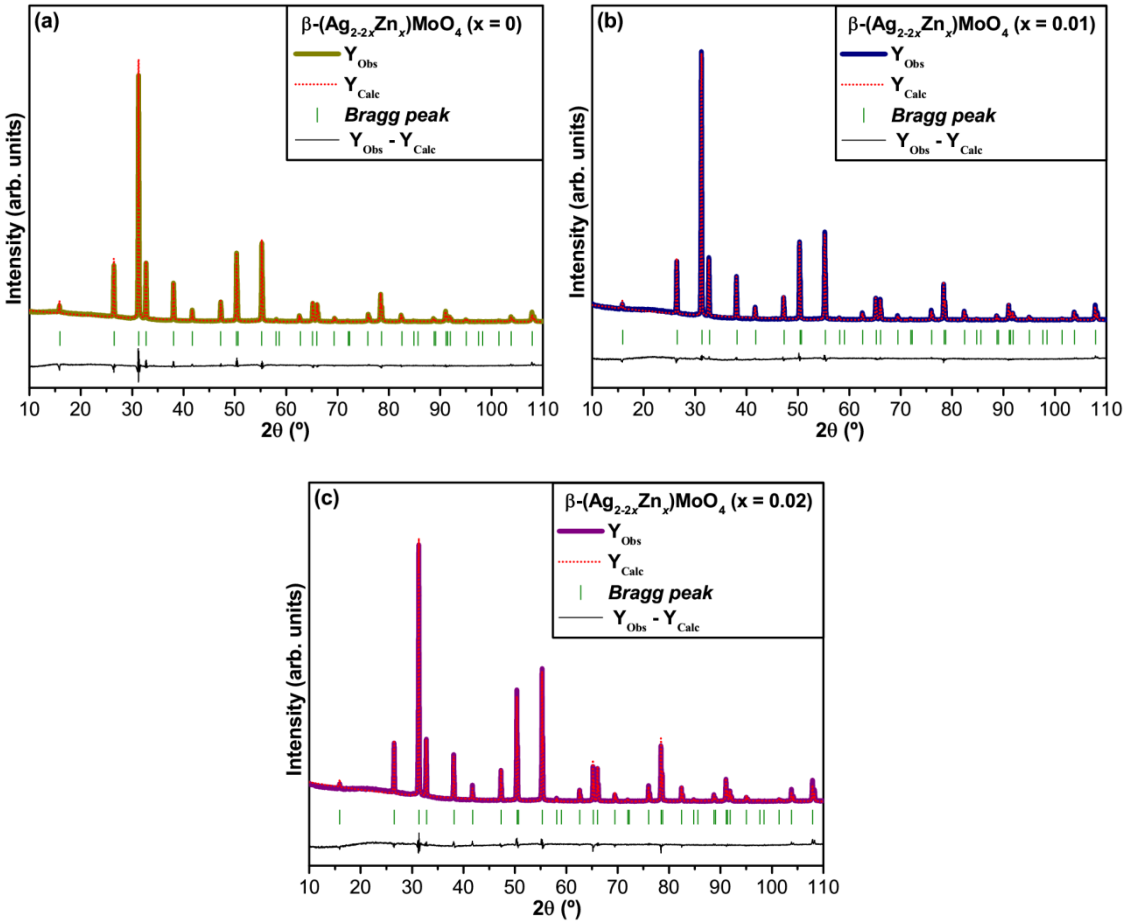

Fig. 3: Rietveld refinement plot of β-$(Ag_{2-2x}Zn_x)MoO_4$ microcrystals with (a) $x = 0$; (b) $x = 0.01$; and (c) $x = 0.02$; synthesized by the ions injection method at 90 ºC for 1 min, respectively.

The experimental lattice parameters, unit cell volume and atomic positions of β–$(Ag_{2-2x}Zn_x)MoO_4$ microcrystals with ($x = 0$; 0.01; and 0.02) obtained experimentally by new synthesis method were calculated using the Rietveld refinement method (CUNHA, F.S. et al, 2015), using the ReX software new version 0.9.0 (BORTOLOTTI, M.; LUTTEROTTI, L.; LONARDELLI, I., 2009; BORTOLOTTI, M.; LONARDELLI, I., 2013), as displayed in Figs. 3(a-c). The Rietveld method is based on the construction of diffraction patterns calculated according to the structural model (WANG, X.; LIAO, L., 2017). The calculated patterns are adjusted to fit the observed patterns and thus provide the structural parameters of the material and the diffraction profile. In this work, the Rietveld method was applied to adjust the atomic positions, lattice parameters, and unit cell volume. The structural refinement was performed indicated the presence of strain lattice and stress (FINGER, L.W.; COX, D.E.; JEPHCOAT, A.P., 1994. The structural refinement quality is generally checked using the *R* values (R_p, R_{exp}, R_{wp}), x^2, and *GoF* (*Goodness of Fit*) (TOBY, B.H., 2006). The difference between the observed and calculated patterns is the best way to judge the success of the Rietveld refinement. However, other parameters with additional functions were applied to find a structural refinement with better quality and reliability. As a general rule, the use of ReX software new version 0.9.0 for a the best Refinement of our samples were performed with the automatic optimization works only a few

parameters are enabled at a time, as trying to optimize too many parameters at once may lead to instabilities in the optimization algorithm and/or location of false minima. This particularly holds for chemical, physical, and atomic properties which have non linear effects on the diffraction model, as atom coordinates and displacement factors. Therefore, the optimized parameters were the scalar factor, 2θ offsets, sample position, background function with Chebyshev polynomial coeffients (C_0, C_1, C_2, and C_3), adjusting the diffraction peaks shape with pseudo-Voigt function, a effective correction of powder diffraction peak due to axial divergence, basic phase, crystal structure, cell parameters (*a, b, c*), angles (α, β, γ), lattice strain, and $U_{isotropic}$ factor (BISH, D.L.; POST, J.E., 1993). All the structural refinement results obtained using the Rietveld method (BORTOLOTTI, M.; LUTTEROTTI, L.; LONARDELLI, I., 2009; BORTOLOTTI, M.; LONARDELLI, I., 2013) were quite consistent with COD-CIF card Nº. 722296 (WANG, X.F. et al, 2014). However, the lower angle region where the most intense peaks are located revealed a major difference. Finally, all refinements illustrated in Figs. 3(a–c) indicate a reasonable correlation between observed and calculated XRD patterns ($Y_{Obs} - Y_{Calc}$ lines), which proves and reinforces the reliability of the experimental results. More details on these obtained data to β-$(Ag_{2-2x}Zn_x)MoO_4$ microcrystals with (x = 0; 0.01; and 0.02) prepared by the ions injection method in a hot solution at 90 ºC in 1 minute with fast cooling by immersion in an ice bath is shown in Table 1(a–c) below:

[(a)]*Atoms*	Wyckoff	Site	S.O.F	x	y	z	U_{iso}
Ag	16*d*	.-3m	1	0.5	0.5	0.5	0.034520
Mo	8*a*	-43m	1	0.125	0.125	0.125	0.029516
O	32*e*	.3m	1	0.234836	0.234751	0.235789	0.033757

[(a)] $a = b = c$ = 9.31957(9) Å, V = 809.12(1)Å³; α = β = γ = 90°, r = 6.17 g/cm³; m/r = 164.58 = cm²/g

R_p (%) = 8.1413, R_{wp} (%) = 10.1763, R_{exp}(%) = 3.5866, χ^2 = 8.0485 and *GoF* = 2.837

[(b)]*Atoms*	Wyckoff	Site	S.O.F	x	y	z	U_{iso}
Ag	16*d*	.-3m	0.979	0.5	0.5	0.5	0.030963
Zn	16*d*	.-3m	0.021	0.5	0.5	0.5	0.029310
Mo	8*a*	-43m	1	0.125	0.125	0.125	0.028068
O	32*e*	.3m	1	0.234823	0.234823	0.234823	0.034939

[(b)] $a = b = c$ = 9.31750(1) Å, V = 808.94(1)Å³; α = β = γ = 90°, r = 6.11 g/cm³; m/r = 162.65 = cm²/g

R_p (%) = 7.0792, R_{wp} (%) = 9.3312, R_{exp}(%) = 3.9334, χ^2 = 5.62781 and *GoF* = 2.3723

[(c)]*Atoms*	Wyckoff	Site	S.O.F	x	y	z	U_{iso}
Ag	16*d*	.-3m	0.968	0.5	0.5	0.5	0.041442
Zn	16*d*	.-3m	0.032	0.5	0.5	0.5	0.038915
Mo	8*a*	-43m	1	0.125	0.125	0.125	0.014974
O	32*e*	.3m	1	0.237408	0.237408	0.237408	0.027793

[(c)] $a = b = c$ = 9.31757(7) Å, V = 808.94(8)Å³; α = β = γ = 90°, r = 6.11 g/cm³; m/r = 162.65 = cm²/g

R_p (%) = 0,089241, R_{wp} (%) = 10.6447, R_{exp}(%) = 3.6857, χ^2 = 8,34112 and *GoF* = 2.8881

Table 1: Data obtained from Rietveld refinements for β-$(Ag_{2-2x}Zn_x)MoO_4$ microcrystals with **(a)** *x*

= 0; (b) x = 0.01; and (c) x = 0.02; synthesized by the ions injection method at 90 ºC for 1 min, respectively.

In these tables, fit parameters (R_p, R_{exp}, R_{wp}, χ^2, and *GoF)* suggest that refinement results are very reliable and consistent with a spinel-type cubic structure. Morever, we can also notice a slight reduction in the value of the lattice parameters and unit cell volume, which is promoted by replacement of Ag^+ by Zn^{2+} ions into the cubic lattice. These Rietveld data are considerable variations in the atomic positions related to the O atoms, while Ag, Zn, and Mo atoms remain fixed in their positions within the cubic structure. This information indicates the existence of distorted octahedral [AgO_6]/[ZnO_6] clusters and undistorted tetrahedral [MoO_4] clusters to the β–($Ag_{2-2x}Zn_x$)MoO_4 structure with (x = 0; 0.01; and 0.02), which arise with different levels of defects and strain lattice.

3.3 Unit Cell Representation Of β-($Ag_{1.96}Zn_{0.02}$)MoO_4 Crystals

Fig. 4 shows the schematic representation for the unit cell of β–($Ag_{2-2x}Zn_x$)MoO_4 microcrystals with (x = 0.02).

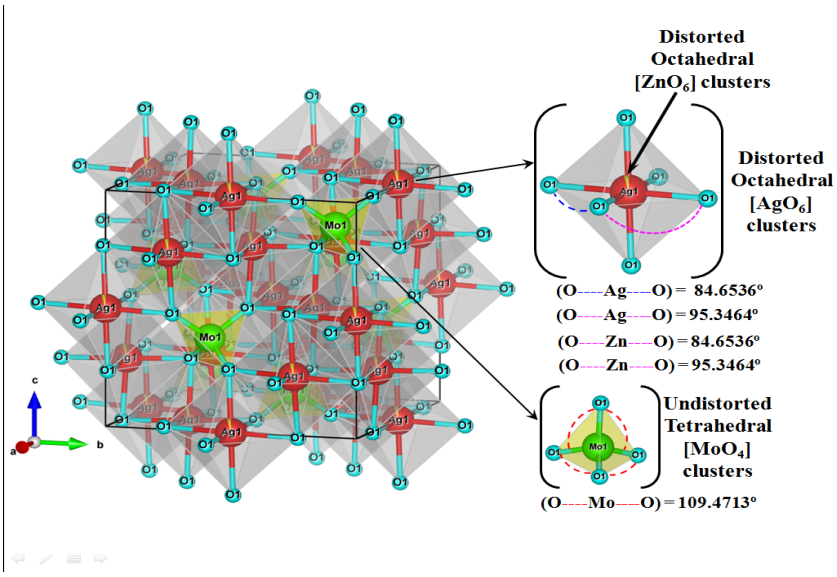

Fig 4: Schematic representation of the unit cell of the β-($Ag_{2-2x}Zn_x$)MoO_4 crystals (x = 0.02) with their respective cluster coordination.

The lattice parameters and atomic positions estimated by means of Rietveld refinements data have been employed to model these structure with the Visualization for Electronic and Structural Analysis (VESTA) program (new version 3.4.6 for Windows-7) (MOMMA, K.; IZUMI, F., 2008; MOMMA, K.; IZUMI, F.,2011). The spinel-type cubic structure of modifired β-($Ag_{1.96}Zn_{0.02}$)MoO_4 crystals is symmylar to pure β-Ag_2MoO_4 crystals, which is characterized by the space group (*Fd3m*) with eight molecular formulae per unit cell (Z = 8) (DONOHUE, J.; SHAND, W., 1947). In these structures, the Ag atoms are coordinated to six O atoms forming distorted octahedral

$[AgO_6]$ clusters with two different bonding angles between (O–Ag–O) in the horizontal plane (*x*, *y*) of the center of the octahedron. Meanwhile, the Mo atoms are coordinated to four O atoms, which result in undistorted tetrahedral $[MoO_4]$ clusters with same bonding angles between (O–Mo–O) (Fig. 4). In principle, our Rietveld refinement data exhibited especially the anisotropic displacement parameters (U_{iso} factor), which are presented previously in Table 1(a-c). As it can be observed clearly in Fig. 1 and Fig. 4.

In addition, our the modified β-$(Ag_{1.96}Zn_{0.02})MoO_4$ crystals, although they were synthesized stoichiometrically and obeying an electronic balance of load compensation, we have noted that the replacement of Ag^+ by Zn^{2+} ions promote a high strain and lattice distortion throughout the crystalline structure, as well as chemical bonds and bonding angles, present different promoting great distortions on octahedral $[AgO_6]$ and $[ZnO_6]$ clusters. Therefore, despite a small percentage of substitution, we have a considerable difference between the electron density of Ag^+ ions (46 electrons) in relation to Zn^{2+} ions (28 electrons), which contributes to a slight retraction in the cell volume as well as a complete distortion in the crystalline lattice, which is composed by the interconnected $[AgO_6]$–$[ZnO_6]$–$[MoO_4]$ clusters. Finally, in Fig. 1 and Fig. 4, we have noticed that the O–Ag–O bond angles were modified from 84.2087º/95.7913º to 84.6536º/95.3464º, while the O–Mo–O binding angles remain practically the same.

3.4 Field Emission Scanning Electron Microscope Analysis Of β-$(Ag_{2-2x}zn_x)MoO_4$ Crystals

Figs. 5(a–f) illustrate FE-SEM images of β-$(Ag_{2-2x}Zn_x)MoO_4$ microcrystals with (x = 0; 0.01; and 0.02) prepared by the ions injection method in a hot solution at 90 ºC in 1 minute with fast cooling by immersion in an ice bath, respectively.

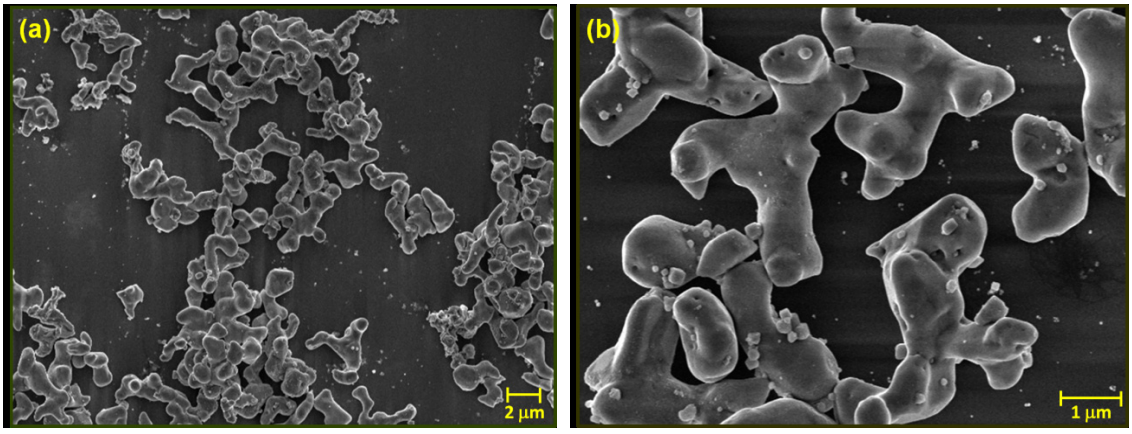

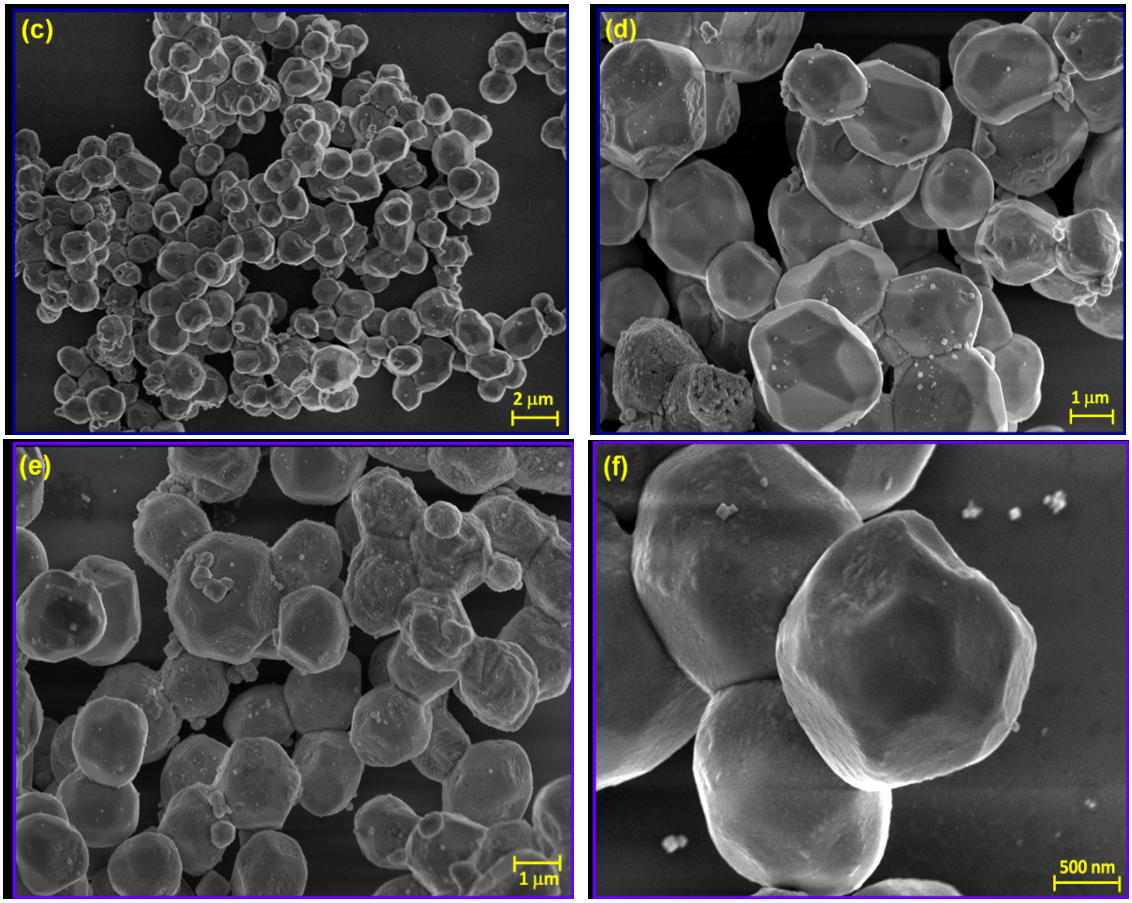

Fig. 5: FE-SEM images of β–($Ag_{2-2x}Zn_x$)MoO_4 microcrystals with (a) $x = 0$; (b) $x = 0.01$; (c) $x = 0.02$, and (d) $x = 0.04$, prepared by the ions injection method, respectively.

As can be seen in Figs. 5 (a,b) it was not possible to obtain a perfect control in the morphology or shape of our pure β-Ag_2MoO_4 crystals. Based on our laboratory experience using deionized water as a solvent. We attribute this inhomogeneous morphology to the high differences in electron density between the Ag^+ and MoO^{2-}_4 complexes ions due to a strong electrostatic attraction between these ions, which results in the formation of the first precipitates of β-Ag_2MoO_4 or nucleation seeds. In our synthesis method, the fast ions injection method in a hot solution at 90 ºC in 1 minute is able to promote localized superheating in the aqueous solution, as well as accelerate solid particles at high speeds. These two phenomena induce a random aggregation between the small particles, due to the increase of the effective collisions, which results in a system composed of several irregular β-Ag_2MoO_4 microcrystals. This behavior can be explained due to the use of fast cooling by immersion in an ice bath. In this case, the average crystal size was estimated using the GNU Image Manipulation Program (GIMP 2.10.10 version for Windows-7) (GIMP 2019). These microcrystals exhibit an average size of about 2.8 µm, with a range from 2.1 µm to 3.7 µm. Moreover, some small β-Ag_2MoO_4 crystals also are observed found, which presents a range from 250 nm to 500 nm. However, it is noted in Figs. 5(c,d), that the effect of (x = 0.01) Zn^{2+} ions is sufficiently able to promote a large morphological modification in pure β–Ag_2MoO_4 microcrystals. The first effect is related to a reduction in the average crystal size, which is clearly observed and the second effect that is

assigned to an increase in the rate of aggregation between the small crystals, which its possible visualize by the several porous formed at the crystal surface. Moreover, the FE–SEM images analysis of these β–($Ag_{1.98}Zn_{0.01}$)MoO_4 microcrystals revealed an average size at around 2.3 μm, with a range from 1.4 μm to 3.2 μm.

Finally, in Figs. 5(e,f) we can be noted the presence of several pores and roughness on the surface of irregular β–($Ag_{2-2x}Zn_x$)MoO_4 microcrystals with (x = 0.02). In this way, we attributed that occurs a mass transport between the several nanocrystals in contact. As a consequence of this mechanism, the formation of β–($Ag_{1.96}Zn_{0.02}$)MoO_4 microcrystals with well defined shapes is not possible by our synthesis methodology employing deionized water as solvent. Despite the polydisperse nature, ideal thermodynamic conditions for the anisotropic growth of some few convex polyhedral crystals enclosed by high index facets was achieved. The microcrystals present an average crystal size of approximately 1.9 μm, with a range from 1.3 μm to 2.7 μm. Therefore, these observations clearly indicate that a more elaborate control of the synthesis conditions, such as temperature, ion concentration, and solvents are important parameters in the morphologic control of β–Ag_2MoO_4 crystals.

3.5 Ultraviolet–Visible Spectroscopy Analyses Of β-($Ag_{2-2X}zn_x$)MoO_4 Crystals

The optical band gap energy (E_{gap}) was calculated using the Kubelka–Munk equation (2) (KUBELKA, P.; MUNK-AUSSI, F., 1931), which is based on the transformation of diffuse reflectance measurements and can estimate E_{gap} values with good accuracy (MORALES, A.E.; MORA, E.S.; PAL, U., 2007). Particularly, it is used in limited cases of infinitely thick samples. The Kubelka-Munk equation (2) for any wavelength is described by:

$$\mathrm{F}(R_\infty) = \frac{(1-R_\infty)^2}{2R_\infty} \cong \frac{k}{s} \qquad (2)$$

where, $F(R_\infty)$ is the Kubelka-Munk function or absolute reflectance of the sample, R_∞ is the reflectance, k is the molar absorption coefficient and s is the scattering coefficient. In our case, barium sulfate ($BaSO_4$) was adopted as the standard sample in reflectance measurements: $R_\infty = R_{sample}/R\mathrm{BaSO_4}$. In a parabolic band structure, the optical band gap and absorption coefficient of semiconductor oxides (SMITH, R.A., 1978) can be calculated using equation (3):

$$\alpha h\nu = C_1(h\nu - E_{gap})^n \qquad (3)$$

where, α is the linear absorption coefficient of the material, $h\nu$ is the photon energy, C_1 is a proportionality constant, E_{gap} is the optical band gap and n is a constant associated with different kinds of electronic transitions (n = 1/2 for direct allowed, n

= 2 for indirect allowed, n = 3/2 for direct forbidden, and n = 3 for indirect forbidden transitions). According to previous theoretical calculations reported by literature (PERALES, R.L. et al, 2008; SOUSA, G.S. et al, 2019) to β–Ag_2MoO_4 microcrystals exhibit an optical absorption spectrum governed by indirect electronic transitions. This means that after the electronic absorption process, electrons located in minimum energy states in the conduction band (CB) are able to go back to maximum energy states in the valence band (VB) at different point in the Brillouin zone (GOUVEIA, A.F. et al, 2014; SOUSA, G.S. et al, 2019). Based on this information, E_{gap} for the β–$(Ag_{2-2x}Zn_x)MoO_4$ microcrystals with (x = 0; 0.01; 0.02 and 0.04) were calculated using n = 2 in equation (3). Finally, using the absolute reflectance function described in equation (2) with $k = 2\alpha$, we obtain the modified Kubelka–Munk equation as indicated in equation (4):

$$[\mathrm{F}(\mathrm{R}_\infty)h\nu)^{0.5} = C_2\left(h\nu - E_{gap}\right) \tag{4}$$

Therefore, finding the $F(R_\infty)$ value from equation (2) and plotting a graph of $[F(R_\infty)h\nu]^{0.5}$ against $h\nu$, E_{gap} values were calculated for the β–$(Ag_{2-2x}Zn_x)MoO_4$ microcrystals with (x = 0; 0.01; and 0.02) by extrapolating the linear portion of the UV–Vis curves.

Figs. 6(a–c) illustrate the UV–Vis spectra for β–$(Ag_{2-2x}Zn_x)MoO_4$ microcrystals with (x = 0; 0.01; and 0.02) prepared by the ions injection method in a hot solution at 90 ºC in 1 minute with fast cooling by immersion in an ice bath, respectively.

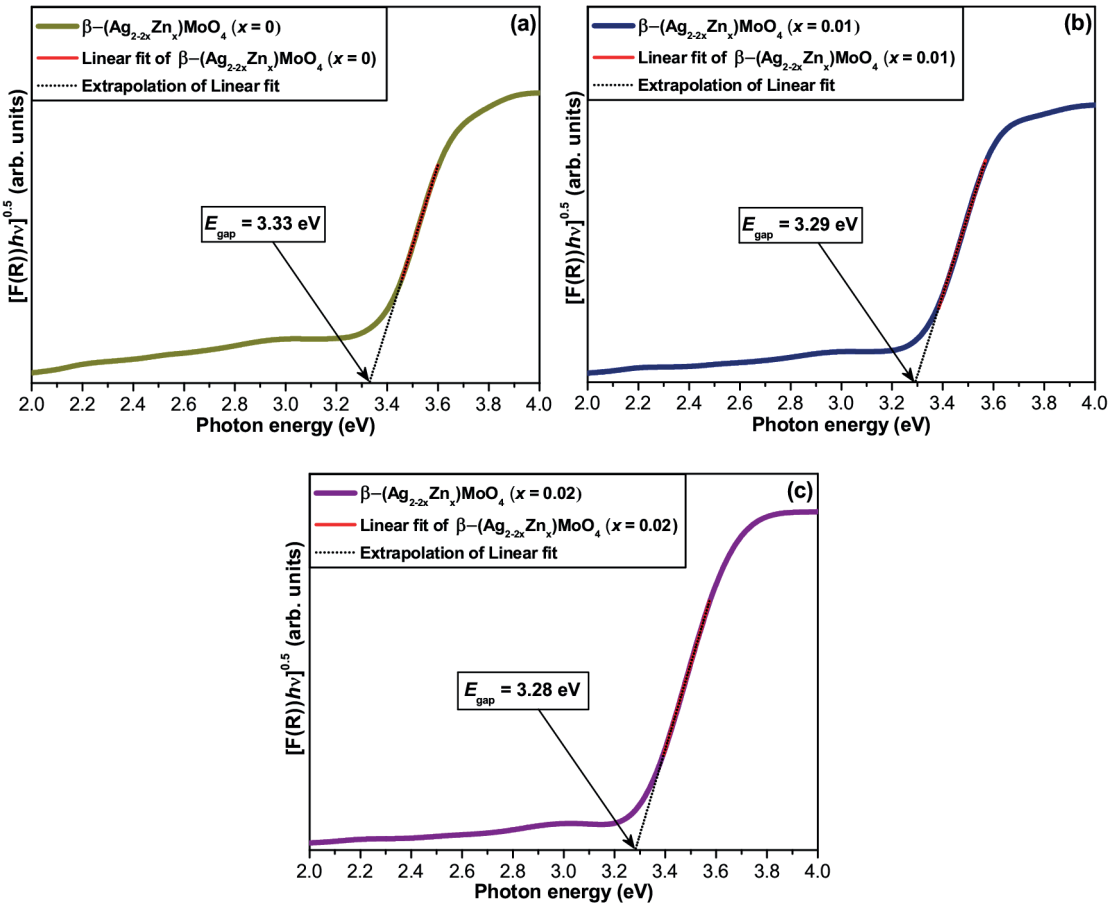

Fig. 6: UV–Vis spectra in diffuse reflecante mode of β–$(Ag_{2-2x}Zn_x)MoO_4$ microcrystals with (a) x = 0; (b) x = 0.01; and (c) x = 0.02, synthesized by the ions injection method at 90 ºC for 1 min, respectively.

As it can be observed in Figs. 6(a–c), the profile of the UV–Vis spectra for our β–$(Ag_{2-2x}Zn_x)MoO_4$ microcrystals with (x = 0; 0.01; and 0.02) indicate an optical behavior typical for structurally ordered crystalline materials. The synthesized pure β–Ag_2MoO_4 microcrystals at same experimental condictions exhibits a indirect optical band gap in the recente literature (FERREIRA, E.A.C. et al, 2019). Moreover, we have noted a slight decreasing in the E_{gap} values (from 3.33 to 3.28 eV), with the replacement of Ag^+ by Zn^{2+} ions into the cubic lattice. Although the E_{gap} values estimated by UV–Vis measurements is considered qualitative and semi-quantitative, the calculated results imply that the microcrystals have distinct types and concentrations of structural and surface defects, such as oxygen vacancies, distortions on the O–Ag–O bonds presents main on octahedral [AgO_6] clusters. The these defects or arise from the crystal formation, growth processes, which were affected by the replacement of Ag^+ by the Zn^{2+} ions into the cubic lattice. Therefore, these defects due to symmetry break are responsible by the lattice polarization, resulting in the presence of intermediary energy levels within the band gap (SOUSA, G.S. et al, 2019). In addition, this table also shows a comparative between the E_{gap} values obtained in this work with those reported in the literature. According to earlier reports (LI, Z.Q.; CHEN, X.T.; XUE, Z.L., 2013; SANTANA, Y.V.B. et al, 2014; SILVA, M.D.P. et al, 2016), pure β–Ag_2MoO_4 microcrystals, powders, or crystals present a broad experimental optical band gap ranging from 3.03 eV to 3.38 eV. As it can be observed in Figs. 6(a-c), we attrubuted that these small changes in E_{gap} values can be related to presence of intermediary energy levels between the VB and CB, since the exponential optical absorption edge and E_{gap} are controlled by the degree of structural order-disorder in the lattice. The slight decrease in E_{gap} values can be attributed to structural defects at medium range and local bond distortions which yield localized electronic levels within the forbidden band gap. A smaller (E_{gap} = 3.23 eV) was detected for β–$(Ag_{1.96}Zn_{0.02})MoO_4$ microcrystals synthesized by the ions injection method at 90 ºC for 1 min, which suggests a high concentration of defects in the cubic lattice (see Fig 4).

3.6 Photocatalytic Properties Analyses Of β-$(Ag_{2-2x}zn_x)MoO_4$ Crystals

Fig. 7(a) displays the photolysis process of the RhB cationic dye solutions, while the Figs. 7(c–d) show the PC degradation of RhB dyes by the β–$(Ag_{2-2x}Zn_x)MoO_4$ microcrystals acting as photocatalyst with (x = 0; 0.01; and 0.02) monitored by the temporal changes in the UV–Vis absorbance spectra of the aqueous dye solutions. The Figs. 7(e) displays the absorption percentage of RhB dye under the β–$(Ag_{2-2x}Zn_x)$ MoO_4 microcrystals with (x = 0; 0.01; and 0.02) (off- UV-light). The degradation rates (C_n/C_0) of the RhB dyes without and with β–$(Ag_{2-2x}Zn_x)MoO_4$ catalyst are shown in

Figure 7(f) and their the rate constants (*k*) obtained for the degradation of RhB dyes by crystals catalyst, respectively.

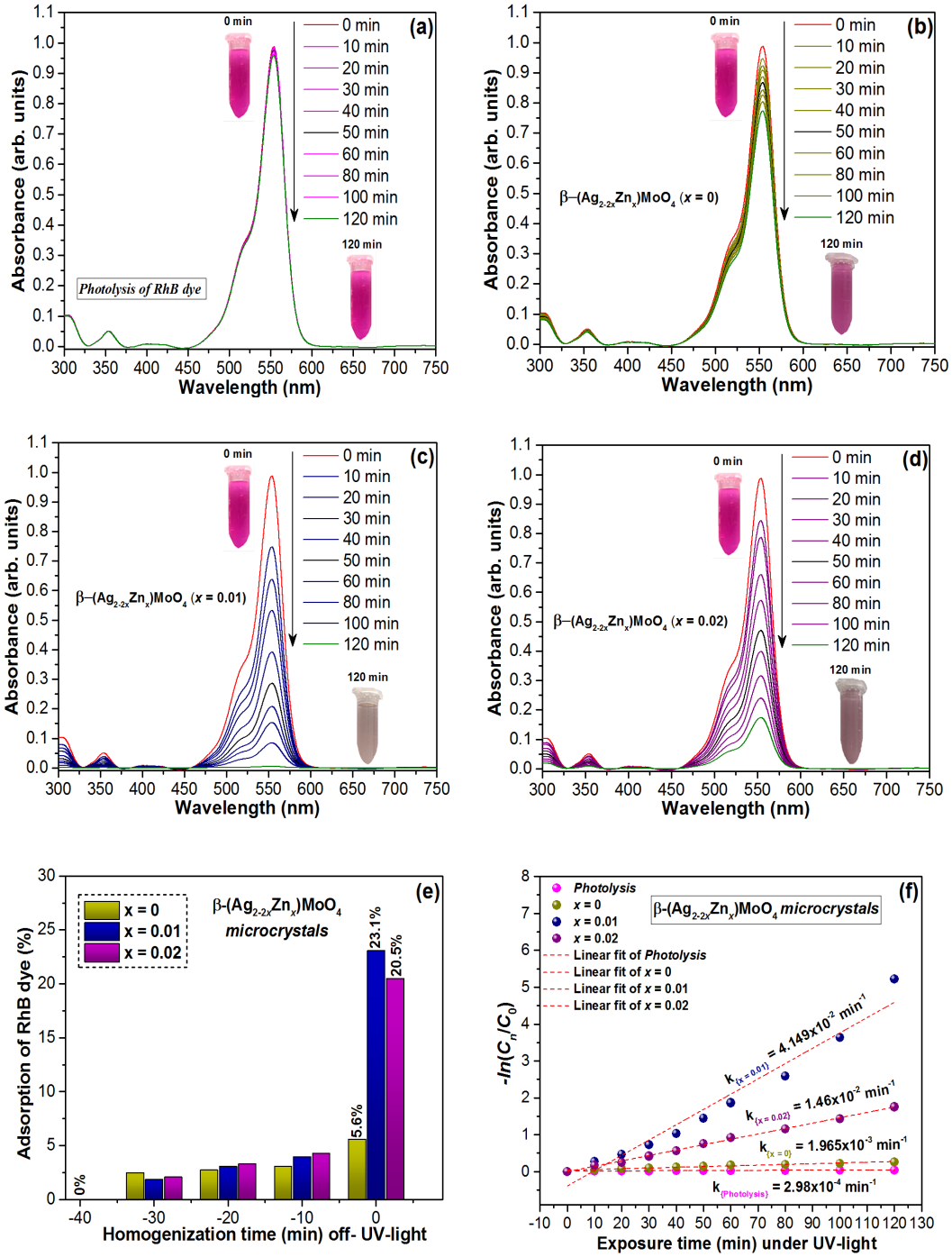

Fig. 7(a) Evolution of UV-Vis absorption spectra after 120 min of illumination without photocatalyst; (b–d) UV-Vis spectra for the photodegradation of RhB dye using β-($Ag_{2-2x}Zn_x$) MoO_4 microcrystals with (x = 0; 0.01; and 0.02). The insets show digital photodegradation photos for RhB dye, (e) Adsorption tests in the dark 30 min before at 10-min intervals for all samples and (f) *First-order kinetics constant* without catalyst or (photolysis) and with our β-($Ag_{2-2x}Zn_x$) MoO_4 microcrystals as catalyst.

Fig. 7(a) indicate an insignificant reduction of approximately 4% of the maximum absorption spectra for the aqueous solutions of RhB dye after 200 min of photolysis, respectively. This behavior indicates a large resistance of the three dyes under UV illumination (JÚNIOR, E.A.A. et al, 2017). As it can be observed in Fig. 7(b), we did

not observe a significant reduction in the concentration of the RhB solution after 120 min of photodiscoloration with the our pure β-Ag_2MoO_4 microcrystals catalyst. Before irradiation, the RhB dye, which is an *N,N,N′,N′*-tetraethylated Rhodamine molecule, had one bandwidth a maximum absorption centered at 543 nm. The photodegradation of the RhB dye occurs due to an oxidative attack via active oxygen species on an *N*-ethyl group (JÚNIOR, E.A.A. et al, 2017). The band moved toward *N,N,N′*-tri-ethylated Rhodamine (λ_{max} = 539 nm), *N,N′*-di-ethylated Rhodamine (λ_{max} = 522 nm), N-ethylated Rhodamine (λ_{max} = 510 nm), and Rhodamine (λ_{max} = 498 nm) species (ZHAO, L. et al, 2007). Therefore, we assumed that our pure β-Ag_2MoO_4 microcrystals catalyst does not have active photocatalytic sites or Lewis basic sites effective for the discoloration or photodegradation of a high percentage of RhB cationic dye after 120 min under UV–light with reduction of approximately 22.7% (see Fig. 7(b)). Moreover, we confirmed that our β–$(Ag_{2-2x}Zn_x)MoO_4$ microcrystals with (x = 0.01) is the most efficient photocatalyst for the degradation of the MO anionic dye after 120 min under UV–light (see Fig. 7(c)). Moreover, our β–$(Ag_{2-2x}Zn_x)MoO_4$ microcrystals with (x = 0.02) exibith a satifactionty rate of discoloration or photodegradation of RhB dye. This behavior can be expliaed by performed a homogenization of this system, 30 min before of starting the PC measurements to reach at adsorption-desorption equilibrium (solid-liquid). Thus, we found the adsorption behavior of all our microcrystals, where the β–$(Ag_{1.98}Zn_{0.01})MoO_4$ catalyst microcrystals has a high percentage of adsorption, as shown in Fig. 7(e). Finally, the equation(1) is generally used for a photocatalytic degradation process if the initial concentration of the organic pollutant is low (1×10^{-5} mol.L^{-1}). According to equation (1), a plot of [$-\ln(C_n/C_0)$] as a function of *t* gives a straight line where the slope is *k (First-order kinetics constant)*. As it can be noted in Fig. 7(f), our β–$(Ag_{2-2x}Zn_x)MoO_4$ photocatalyst microcrystals with (*x* = 0.01 and 0.04) was more effective and efficient for the degradation of RhB cationic dye, than our pure β–Ag_2MoO_4 microcrystals, as shown in (inset Fig. 7(f) the rate constants to our β–$(Ag_{2-2x}Zn_x)MoO_4$ photocatalyst microcrystals with (*x* = 0; 0.01; and 0.02) and in the absence of a catalyst only for the photolysis process of RhB dyes are very small ($k_{\{Photolysis\}} = 2.98\times10^{-4}$ min^{-1}), which indicates that there is no significant degradation of this organic dyes due to high strength and stability. Moreover, in Fig. 7(f) its possible note a very significant improvement in photocatalytic performance for β–$(Ag_{2-2x}Zn_x)MoO_4$ microcrystals with (x = 0.01; and 0.02), which we have found that the $k_{\{x = 0.01} = 4.149\times10^{-2}$ $min^{-1}_{\}}$ value is approximately 139.23 times higher than $k_{\{Photolysis*\}}$.

4 I CONCLUSION

In summary, in this book chapter, we have successfully obtained for the first time in the literature the β–$(Ag_{2-2x}Zn_x)MoO_4$] microcrystals with (*x* = 0; 0.01; and 0.02) by the ions injection method in a hot solution at 90 ºC in 1 minute with fast cooling by immersion in an ice bath. XRD patterns and Rietveld refinement data indicated that

all the crystals have a pure phase related to spinel-type cubic structure with the space group (*Fd3m*) and point-group symmetry (O^7_h). Rietveld refinement data confirmed the presence of distorted octahedral [AgO_6]/ [ZnO_6] clusters and undistorted tetrahedral [MoO_4] clusters. FE-SEM images indicated that the replacement of Ag^+ by the Zn^{2+} ions promotes a considerable change of shape, growth process and appearance of pores on the crystal surfaces. UV–Vis spectra shown a slight differences in E_{gap} values were caused by the replacement of Ag^+ by the Zn^{2+} ions, which promotes the formation of new intermediary electronic levels and profile governed by indirect allowed electronic transitions. These new energetic states originated from the defects electronic related to Zn 3*d* orbitals. Finally, we have found good photocatalytic performance of β–($Ag_{2-2x}Zn_x$)MoO_4 microcrystals to degradation of the RhB cationic dye in up to 120 min under UV–light, resulted in the best photocatalytic performances for the β–($Ag_{2-2x}Zn_x$) MoO_4 microcrystals with (x = 0.01), which are can be atributed to defects specific at the crystal surface and high catalytic performance of pores.

ACKNOWLEDGMENT

The Brazilian authors acknowledge the financial support of the Brazilian research financing institutions CNPq (350711/2012-7; 150949/2018-9; 312318/2017-0; 408036/2018-4), FAPEPI, FAPESP (2012/14004-5), and CAPES.

REFERENCES

ABRAHAMS, S.C.; REDDY, J.M. **Crystal Structure of the Transition-Metal Molybdates. I. Paramagnetic Alpha-$MnMoO_4$.** J. Chem. Phys. 43, p. 2533–2543, 1965.

ARORA, A.K.; NITHYA, R.; MISRA, S. et al. J. **Behavior of silver molybdate at high-pressure**. Solid State Chem. 196, p. 391–397. 2012.

BAI, Y.Y.; LU, Y.; LIU, J.K. J. **An efficient photocatalyst for degradation of various organic dyes: Ag@Ag_2MoO_4–AgBr composite**. Hazard. Mater. 307, p. 26–35, 2016.

BELTRÁN, A.; GRACIA, L.; LONGO, E., et al. **First-Principles Study of Pressure-Induced Phase Transitions and Eletronic Properties of Ag_2MoO_4.** J. Phys. Chem. C. 118, p. 3724–3732, 2014.

BI, J.; WU, L.; ZHANG, Y. et al. **Solvothermal preparation, electronic structure and photocatalytic properties of $PbMoO_4$** and $SrMoO_4$. Appl. Catal. B. 91, p. 135–143, 2009.

BISH, D.L.; POST, J.E. **Quantitative mineralogical analysis using the Rietvetd full-pattern fitting method**. Am. Mineral. 78, p. 932–940, 1993.

BORTOLOTTI, M.; LONARDELLI, I. **ReX.Cell: a user-friendly program for powder diffraction indexing**. J. Appl. Cryst. 46, p. 259-261, 2013.

BORTOLOTTI, M.; LUTTEROTTI, L.; LONARDELLI, I. **ReX: a computer program for structural analysis using powder diffraction data**. J. Appl. Cryst. 42, p. 538-539, 2009.

BROWN, S.; MARSHALL, A.; HIRST, P. **The growth of single crystals of lead molybdate by the Czochralski technique**. Mater. Sci. Eng.173, p. 23–27, 1993.

CAVALCANTE, L.S.; MORAES, E.; ALMEIDA, M.A.P. et al. **A combined theoretical and experimental study of electronic structure and optical properties of β-$ZnMoO_4$** microcrystals. Polyhedron. 54, p. 13–25, 2013.

COIMBRA, D.W.R.; CUNHA, F.S.; SCZANCOSKI, J.C. et al. **Structural refinement, morphology and photocatalytic properties of β-$(Ag_{2-2x}Zn_x)MoO_4$ microcrystals synthesized by the sonochemical method**. J. Mater. Sci. Mater. in Electron. 30, p. 1322–1344, 2019.

CUI, X.; YU, S.H.; LI, L. et al. **Selective Synthesis and Characterization of Single-Crystal Silver Molybdate /Tungstate Nanowires by a Hydrothermal Process**.. Chem. Eur. J. 10, p. 218–223, 2004.

CUNHA, F.S.; SCZANCOSKI, J.C.; NOGUEIRA, I.C. et al. **Structural, morphological and optical investigation of β-Ag_2MoO_4 microcrystals obtained with different polar solvents.** CrystEngComm. 17, p. 8207–8211, 2015.

CUTRONI, M.; FEDERICO, M.; MANDANICI, A. et al. **A.C. conductivity in $(AgI)_{1-x(Ag2}MoO_4)_x$** ionic glasses in the 77–300 K temperature region. Solid State Ionics. 113–115, p. 681–683, 1998.

DONOHUE, J.; SHAND, W. **The determination of the interatomic distances in silver molybdate, Ag_2MoO_4**. J. Am. Chem. Soc. 69**,** p. 222–223, 1947.

FABBRO, M.T.; FOGGI, C.C.; SANTOS, L.P.S. et al. **Synthesis, antifungal evaluation and optical properties of silver molybdate microcrystals in different solvents: a combined experimental and theoretical study**. Dalton Trans. 45, p. 10736–10743, 2016.

FERREIRA, E.A.C.; NETO, N.F. A.; BOMIO, M.R.D. et al. **Influence of solution pH on forming silver molybdates obtained by sonochemical method and its application for methylene blue degradation**. Ceram. Internat. 45, p.11448–11456, 2019.

FIGUEIREDO, A.T.; LAZARO, S.; LONGO, E. et al. **Correlation among order–disorder, electronic levels, and photoluminescence in amorphous ct:Sm**. Chem. Mater. 18, p. 2904-2911, 2006.

FINGER, L.W.; COX, D.E.; JEPHCOAT, A.P. **A correction for powder diffraction peak asymmetry due to axial divergence**. J. Appl. Cryst. 27, p. 892-900, 1994.

FODJO, E.K.; LI, D.W.; MARIUS, N.P. et al. **Low temperature synthesis and SERS application of silver molybdenum oxides**. J. Mater. Chem. A. 1, p. 2558–2566, 2013.

GIMP. **GNU IMAGE MANIPULATION PROGRAM.** C2019, Home page. Available at: <https://www.gimp.org/>. Accessed on: Jun 2 2019..

GONG, Q.; QIAN, X.; MA, X. et al. **Large-Scale Fabrication of Novel Hierarchical 3D $CaMoO_4$ e $SrMoO_4$ Mesocrystals via a Microemulsion-Mediated**. Crys. Growth Des. 6, p. 1821–1825, 2006.

GOUVEIA, A.F.; SCZANCOSKI, J.C.; FERRER, M.M., et al. **Experimental and Theoretical Investigations of Electronic Structure and Photoluminescence Properties of b-Ag_2MoO Microcrystals.** Inorg. Chem. 53, p. 5589–5599, 2014.

GUPTA, S.K.; GHOSH, P.S.; SUDARSHAN, K. et al. **Multifunctional pure and Eu^{3+}** doped β-**Ag_2MoO_4: photoluminescence, energy transfer dynamics and defect induced** properties. Dalton Trans. 44, p. 19097–19110, 2015.

HASHIM, M.; HU, C.; CHEN, Y. et al. **Synthesis, characterization, and optical properties of $Ag_2Mo_2O_7$** nanowires. Phys. Status Solidi A. 208, p. 1937–1941, 2011.

JIAO, Z.; ZHANG, J.; LIU, Z. et al. **Ag/AgCl/Ag_2MoO_4 composites for visible-light-driven photocatalysis**. J. Photochemistry and Photobiology A: Chemistry. 371, p. 67-75, 2019.

JUAREZ, J.C.; MORALES, R. **Reduction Kinetics of Ag_2MoO_4** by Hydrogen. Metallurg. Mater. Trans. B. 39, p. 738–745, 2008.

JÚNIOR, E.A.A.; NOBRE, F.X.; SOUSA, G.S.; et al. **Synthesis, growth mechanism, optical properties and catalytic of ZnO microcrystals obtained *via* hydrothermal processing**. RSC Adv. 7, p. 24263-24281, 2017.

KOKULNATHAN, T.; CHEN, T.W.; CHEN, S.M. et al. **Hydrothermal synthesis of silver molybdate/reduced graphene oxide hybrid composite: An efficient electrode material for the electrochemical detection of tryptophan in food and biological samples.** Composites Part B: Engineering. 169, p. 249-257, 2019.

KOMARNENI, S.; ROY, R.; LI, Q.H. **Microwave-hydrothermal synthesis of ceramic powders**. Mater. Res. Bull. 27, p. 1393–1405, 1992.

KUBELKA, P.; MUNK-AUSSI, F. **Ein Beitrag Zur Optik Der Farbanstriche**. Z. Tech. Phys.12, p. 593–601, 1931.

LEI, F.; YAN, B.; CHEN, H.H. et al. **Surfactant-Assisted Hydrothermal Synthesis, Physical Characterization, and Photoluminescence of $PbWO_4$**. Cryst. Growth Des. 9**,** p. 3730–3736, 2009.

LI, L.; LENG, Z.; ZI, W. et al. **Hydrothermal Synthesis of $SrMoO_4$: Eu^{+3}, Sm^{+3} Phosphors and their Enhanced Luminescent Properties Through Energy Transfer**. Electron. Mater. 43, p. 2588–2596, 2014.

LIU, E.; GAO, Y.; JIA, J., et al. **Friction and wear behaviors of Ni-based composites containing graphite / Ag_2MoO_4 lubricats**. Trib. Lett. 50, 313–322, 2013.

LI, Z.Q.; CHEN, X.T.; XUE, Z.L. **Microwave-assisted hydrothermal synthesis of cube-like Ag-Ag_2MoO_4 with visible-light photocatalytic activity**. Sci. China Chem. 56, p. 443-450, 2013.

LI, Z.Q.; CHEN, X.T.; XUE, Z.L. **Microwave-assisted hydrothermal syntesis of cube-like Ag-Ag_2MoO_4 with visible-light photocatalytic activity**. Sci. China Chem. 56, p. 443–450, 2013.

MANDANICI, A.; RAIMONDO, A.; CUTRONI, M., et al. **Thermal expansion of silver iodide-silver molybdate glasses at low temperatures**. J. Chem. Phys. 130, p. 204508–204514, 2009.

MARQUES, A.P.A.; MELO, D.M.A.; PASKOCIMAS, C.A., et al. **Photoluminescent $BaMoO_4$** nanopowders prepared by complex polymerization method (CPM). J. Solid State Chem. 179, p. 671–678, 2006.

MEENA, S.K.; HEDA, N.L.; ARORA, G. et al. **Performance of hybrid exchange-correlation potential for photocatalytic silver chromate and molybdate: LCAO theory and Compton spectroscopy**. Phys. B. 560, p. 236–243, 2019.

MOMMA, K.; IZUMI, F. **VESTA: a three-dimensional visualization system for electronic and structural analysis**. J. Appl. Crystallogr. 41, p. 653–658, 2008.

MOMMA, K.; IZUMI, F. **VESTA 3 for three-dimensional visualization of crystal, volumetric and**

morphology data. J. Appl. Crystallogr. 44, p. 1272–1276, 2011.

MORALES, A.E.; MORA, E.S.; PAL, U. **Use of diffuse reflectance spectroscopy for optical characterization of un-supported nanostructures**. Rev. Mex. Fís. S. 53, p. 18–22, 2007.

MOURA, J.V.B.; FILHO, J.G.S.; FREIRE, P.T.C. et al. **Phonon properties of β-Ag_2MoO_4: Raman spectroscopy and *ab initio*** calculations.Vibrat. Spectrosc. 86, p. 97–102, 2016.

NOGUEIRA, I.C.; CAVALCANTE, L.S.; PEREIRA, P.F.S.; et al. **Rietveld refinement, morphology and optical properties of $(Ba_{1-x}Sr_x)MoO_4$ crystals.** J. Appl. Cryst. 46, p. 1434–1446, 2013.

NG, C.H.B.; FAN, W.Y. **Crystal origami: Preparation of β-Ag_2MoO_4 concave and convex crystals with high-index facets**. Chem Nano Mat. 3, p. 178-182, 2017.

NG, C.H.B.; FAN, W.Y. **Uncovering Metastable a-Ag2MoO4 Phase Under Ambient Conditions. Overcoming High Pressure by 2,3-Bis(2-pyridyl)pyrazine Doping**. Cryst. Growth Des. 15, p. 3032–3037, 2015.

PERALES, R.L.; FUERTES, J.R.; ERRANDONEA, D. et al. **A. Segura, Optical absorption of divalent metal tungstates: Correlation between the band-gap energy and the cation ionic radius**. Europhys. Lett. 83, p. 37002–37006, 2008.

RAO, K.S.; VAIDYA, V.G. **Precipitation of silver molybdate from homogeneous solution by use of diamminesilver (I) reagent**. Analyst. 100, p. 512–516, 1975.

RIETVELD, H.M. **A profile refinement method for nuclear and magnetic structures**. J. Appl. Crystallogr. 2, p. 65–71,1969.

RIETVELD, H.M. **Line profiles of neutron powder-diffraction peaks for structure refinement**. Acta Crystallogr. 22, p. 151–152,1967.

RICCI, J.E.; LINKE, W.F. **The Aqueous Solubility of Silver Molybdate and the Ternary Systems Ag_2MoO_4-$AgNO_3$-H_2O and Ag_2MoO_4-Na_2MoO_4-H_2O at 25°**. J. Am. Chem. Soc. 73, p. 3601–3603, 1951.

ROCCA, F.; KUZMIN, A.; MUSTARELLI, et al. **XANES and EXAFS at Mo K-edge in $(AgI)_{1-x(Ag2}MoO_4)_x$** glasses and crystals. Solid State Ionics. 121, p. 189–192, 1999.

RYU, J.H.; YOON, J.W.; LIM, C.S. et al. **Microwave-assisted synthesis of $CaMoO_4$nano-powders by a citrate complex method and its photoluminescence property**. J. Alloys Compd. 390, p. 245–249, 2005.

SANTANA, Y.V.B.; GOMES, J.E.C.; MATOS, L. et al. **Silver molybdate and silver tungstate nanocomposites with enhanced photoluminescence**. Nanomater. Nanotechnol. 4, p. 22-1-22-11, 2014.

SCZANCOSKI, J.C.; CAVALCANTE, L.S.; JOYA, M.R. et al. **$SrMoO_4$** powders processed in microwave-hydrothermal: Synthesis, characterization and optical properties. Chem. Eng. J. 140, p. 632–637, 2008.

SILVA, M.D.P.; GONÇALVES, R.F.; NOGUEIRA, I.C. et al. **Microwave-assisted hydrothermal synthesis of $Ag_2(W_{1-x}Mo_x)O_4$ heterostructures: Nucleation of Ag, morphology, and photoluminescence properties**. Spectrochim. Acta Part A. 153, p. 428-435, 2016.

SINGH, D.P.; SIROTA, B.; TALPATRA, S. et al. **Broom-like and flower-like heterostructures of silver molybdate througt pH controlled self-assembly**. J. Nanopart. Res. 14, p. 781–792, 2012.

SMITH, G.W.; IBERS, J.A. **The crystals structure of cobalt molybdate $CoMoO_4$**. Acta Cryst. 19, p. 269–275, 1965.

SMITH, G.W.; IBERS, J.A. **The crystals structure of cobalt molybdate $CoMoO_4$**. Acta Cryst. 19, p. 269–275, 1965.

SMITH, R.A. **Semiconductors**. Cambridge University Press: London, 2nd. p. 1–535, 1978.

SOMIYA, S.; ROY, R. **Hydrothermal synthesis of fine oxide powders**. Mater. Sci. Bull. 23, p. 453–460, 2000.

SOUZA, E.L.S.; DALMASCHIO, C.J.; FILHO, M.G.R., et al. **Formatex, Microscopy: advances in scientific research and education**. 2, p. 894–902, 2014.

SOUSA, G.S.; NOBRE, F.X.; JÚNIOR, E.A.A. et al. **Hydrothermal synthesis, structural characterization and photocatalytic properties of β-Ag_2MoO_4** microcrystals: Correlation between experimental and theoretical data. Arabian J. Chem. 2019. in press DOI:10.1016/j.arabjc.2018.07.011

SUDARSHAN, S.S; GUPTA, K.; SONAWANE, K. et al. **Room temperature synthesis, concentration quenching study and defect formation in β-Ag_2MoO_4:Dy^{3+}- photoluminescence and positron annihilation spectroscopy**. J. Lumin. 212, p. 293-299, 2019.

SUTHANTHIRARAJ, S.A; PREMCHAND, Y.D. **Molecular structural analysis of 55 mol% CuI-45 mol% Ag_2MoO_4** solid electrolyte using XPS and laser raman techniques. Ionics. 10, p. 254–257, 2004.

TAWDE, D.; SRINIVAS, M.; MURTHY, K.V.R. **Effect of lead source and cerium (III) doping on structural and photoluminescence properties of $PbWO_4$** microcrystallites synthesized by hydrothermal method. Phys. Status Solidi A. 208, p. 803–807, 2011.

THÉODET, M.; QUILFEN, C.; MARTÍNEZ, C. et al. **Continuous supercritical synthesis of unsupported and high specific surface area catalyst precursors for deep-hydrodesulfurization**. J. Supercrit. Fluids. 117, p. 252–259, 2016.

TIAN, G.; SUN, S. **Additive induced morphology changes of nano-crystalline $SrWO_4$**. Cryst. Res. Technol. 46, p. 188–194, 2011.

TOBY, B.H. **Rfactors in Rietveld analysis: How good is good enough?**. Powder Diffraction. 21, p. 67–70, 2006.

WENDA, E. **High Temperature Reactions in the MoO_3-Ag_2O System**. J. Therm. Anal. Calor. 53, p. 861–870, 1998.

WENDA, E. **Phase diagram of the V_2O_5-MoO_3-Ag_2O system II. Phase diagram of MoO_3-Ag_2O system.** J. Therm. Anal. Calor. 36, p. 1417–1427, 1990.

WANG, P.; HUANG, B.; QIN, X. et al. **Whangbo, Ag/AgBr/WO_3.3H_2O: visible-light photocatalyst for bacteria destruction**. Inorg. Chem. 48, p. 10697–10702, 2009.

WANG, X.; LIAO, L. **Rietveld Structure Refinement of Cu-Trien Exchanged Nontronites**. Front. In Chem. 6, p. 558-1-558-8, 2017.

WANG, X.F.; PENG, G.H.; LI, N. et al. **Hydrothermal synthesis and luminescence properties of 3D walnut-like $CaMoO_4$:Eu^{3+}** red phosphors. J. Alloys Compd. 599, p. 102–107, 2014.

WANG, W.S.; ZHEN, L.; XU, C.Y. et al. **Room Temperature Synthesis, Growth Mechanism,**

Photocatalytic and Photoluminescence Properties of Cadmium Molybdate Core-Shell Microspheres. J. Phys. Chem. B. 110, p. 23154–23158, 2009.

WU, M.; LY, J.; WANG, T. et al **Ag_2MoO_4 nanoparticles encapsulated in g-C_3N_4 for sunlight photodegradation of pollutants**. Catalysis Today. 315, p. 205-212, 2018.

WYCKOFF, R.W.G. J. **The crystal structure of silver molybdate**. Am. Chem. Soc. 44, p. 1994–1998, 1922.

XUE, Y.N.; SUN, Y.S.; LIU, J.K.. et al. **Construction, enhanced visible-light photocatalytic activity and application of multiple complementary Ag dots decorated onto Ag_2MoO_4/AZO hybrid nanocomposite**. Res. Chem. Intermed. 45, p. 873–892, 2019.

YADAVA, Y.P.; SINGH, R.A. **Electrical transport properties of iron (II) molybdate**. J. Mater. Sci. 21, p. 2825–2829, 1986.

ZHAO, L.; LI, C.; LIU, X. et al. **Highly enhanced degradation of dye with well-dispersed TiO_2 nanoparticles under visible irradiation**. 440, p. 281-286, 2007.

SOBRE O ORGANIZADOR

CLEBERTON CORREIA SANTOS- Graduado em Tecnologia em Agroecologia, mestre e doutor em Agronomia (Produção Vegetal). Tem experiência nas seguintes áreas: agricultura familiar, indicadores de sustentabilidade de agroecossistemas, uso e manejo de resíduos orgânicos, propagação de plantas, manejo e tratos culturais em horticultura geral, plantas medicinais exóticas e nativas, respostas morfofisiológicas de plantas ao estresse ambiental, nutrição de plantas e planejamento e análises de experimentos agropecuários.

(E-mail: cleber_frs@yahoo.com.br) – ORCID: 0000-0001-6741-2622

ÍNDICE REMISSIVO

A

B

C

D

E

G

H

I

M

N

O

P

R

S

Agência Brasileira do ISBN
ISBN 978-85-7247-621-8
9 788572 476218